nature portfolio

https://doi.org/10.1038/s41586-024-08543-1

Supplementary information

Observation of an ultra-high-energy cosmic neutrino with KM3NeT

In the format provided by the authors and unedited

Supplementary Information for "Observation of an Ultra-High-Energy Cosmic Neutrino with KM3NeT"

The KM3NeT Collaboration

1 Comparison with existing measurements, limits, and models

The expected number of events in KM3NeT/ARCA is a convolution of the all-flavour exposure $\mathcal{E}^{\mathrm{KM3NeT}}$ (see Methods) and the considered per-flavour $\nu + \bar{\nu}$ differential flux Φ:

$$n_{\mathrm{expected}}^{\mathrm{KM3NeT}} = \int \mathcal{E}^{\mathrm{KM3NeT}}(E) \times \Phi(E)\mathrm{d}E. \tag{1}$$

The exposure is computed selecting events with log-likelihood ratio larger than 500 and $\mathcal{N}_{\mathrm{trig}}^{\mathrm{PMT}}$ larger than 1500. The integration bounds may be chosen either to cover the full energy range or to correspond to the central 90% neutrino energy range associated with KM3-230213A.

Supplementary Table 1 collects the expected number of events in KM3NeT/ARCA when considering some IceCube best-fit single power-law flux measurements at lower energies and various diffuse models. In particular, the table highlights that the KM3-230213A observation is rather improbable in the scenario where the true neutrino spectrum was a simple extrapolation of IceCube HESE single power-law best fit, therefore hinting at the emergence of a new component in the flux.

2 Evidence for secondary cascades

The muon trajectory is reconstructed using the first hit observed on each PMT, assuming that the light is emitted from the muon at the Cherenkov angle θ_C. Indeed, at any position in the detector, the earliest photons are those that are from the muon under this angle.

In KM3-230213A, the vast majority of the light is not directly induced by the muon, but by secondary electron-positron cascades that are created along its path. In these cascades, many particles are collinear with the muon and Cherenkov photons are therefore preferentially emitted at θ_C, allowing an accurate reconstruction of the muon trajectory using the first hits detected on each PMT. Electron-positron cascades initiated by the muon also contain non-collinear particles, which emit photons in other directions. For large, stochastic energy losses resulting in energetic cascades, these can be detected by studying photons arriving later than those emitted at θ_C.

The scattering length is large in seawater and photons may be assumed to travel straight from the muon trajectory to the PMT even at large distances in the instrumented volume. The point of emission along the trajectory can then be computed from the time of detection. Adopting the same notation as in Methods, if the photon is emitted at a distance z along the trajectory at position $\vec{w} = \vec{p_0} + z\vec{d}$, the detection time is given by

$$t = t_0 + z/c + |\vec{q} - \vec{w}|/v_g. \tag{2}$$

Solving for z leads to a quadratic equation, which has two solutions corresponding to an emission before and after the Cherenkov emission. The latter case dominates as the former would require the photons to travel large distances through water.

The distribution of the computed emission points of the detected photons is shown in Supplementary Fig. 1. For this figure, as well as for Supplementary Fig.2, all hits are used; not only the first hits on each PMT as is done in the reconstruction and the Extended Data. Three distinct peaks are visible at $z = 199$, 297, and 477 m. At these positions along the trajectory excess photons have been emitted, which indicates the production of discrete high-energy cascades due to stochastic energy losses of the muon. It has been checked that the peaks are not artifacts of the detector geometry by observing that simulations show a variety of peaks at different locations.

A fraction of the detected photons can thus be associated with each one of the three secondary cascades. This is illustrated in Supplementary Fig. 2, where the detected hits are displayed as a function of their time of occurrence and of the vertical position of the PMT along the detection line. Depending on the distance from the detection line to the muon trajectory and to each of the cascades, and on the amount of saturation of the PMTs, the hits from the three cascades can be distinguished.

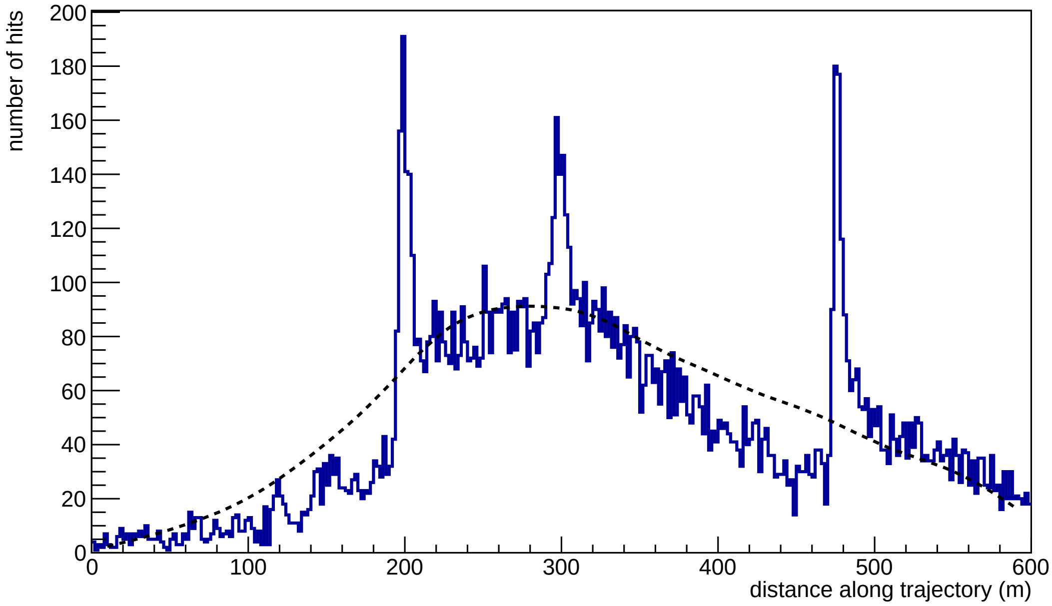

Supplementary Figure 1: Distribution of the computed emission point of photons in KM3-230213A along the reconstructed muon trajectory, represented by the distance to $\vec{p}_0$, the location of the muon at $t = t_0$, as described in the text. To indicate the effect of the detector acceptance, the dashed line shows the average expectation, obtained from simulations of 100 PeV muons with the same direction and position as KM3-230213A.

Supplementary Table 1: Expected number of track events (with the event selection reported in the text) in 335 days of analysed ARCA data in the 19 and 21 detection-line configuration, considering a variety of diffuse astrophysical fluxes, in the full energy range of selected events, or only in the most-probable energy range for KM3-230213A. The different sections report the results for: IceCube single power-law best fits extrapolated to higher energies for different samples, i.e. HESE, NST, and Enhanced Starting Track Event Selection (ESTES); expectations from various cosmogenic models; expectations from source models.

Tested flux	Expected events in ARCA19-21 in full energy range	Expected events in ARCA19-21 in 72 PeV – 2.6 EeV
IceCube single power-law best fits		
IceCube/NST [1]	0.12	0.014
IceCube/ESTES [2]	0.052	3.4×10^{-3}
IceCube/HESE [3]	0.019	5.1×10^{-4}
Cosmogenic models		
Aloisio et al. [4]	0.47	1.6×10^{-2}
Muzio et al. (2023) [5]	0.44	0.25
Ehlert et al. [6]	0.25	0.21
Zhang et al. [7]	0.25	9.5×10^{-2}
Pierre Auger Collaboration [8]	5.3×10^{-2}	3.4×10^{-3}
Muzio et al. (2022) [9]	0.11	1.0×10^{-2}
Boncioli et al. [10]	1.3×10^{-2}	4.1×10^{-3}
Heinze et al. [11]	2.7×10^{-3}	7.7×10^{-4}
Condorelli et al. [12]	2.0×10^{-3}	4.6×10^{-4}
Berat et al. [13]	1.5×10^{-3}	4.0×10^{-4}
Source (transient) diffuse models		
Pulsar (Fang. et al [14])	1.3	0.47
LL-BLLacs (Rodrigues et al. [15])	0.56	0.26
TDE (Winter et al. [16])	0.42	5.5×10^{-2}
LL-GRBs (Boncioli et al. [10])	0.15	2.5×10^{-3}
Sample FSRQ (Rodrigues et al. [17])	1.2×10^{-2}	4.6×10^{-5}
LL-GRB (Tamborra et al. [18])	1.0×10^{-2}	5.9×10^{-4}
Sample LL-BLLac (Rodrigues et al. [17])	5.0×10^{-3}	3.3×10^{-6}
s-GRB (Tamborra et al. [18])	2.8×10^{-6}	6.6×10^{-7}

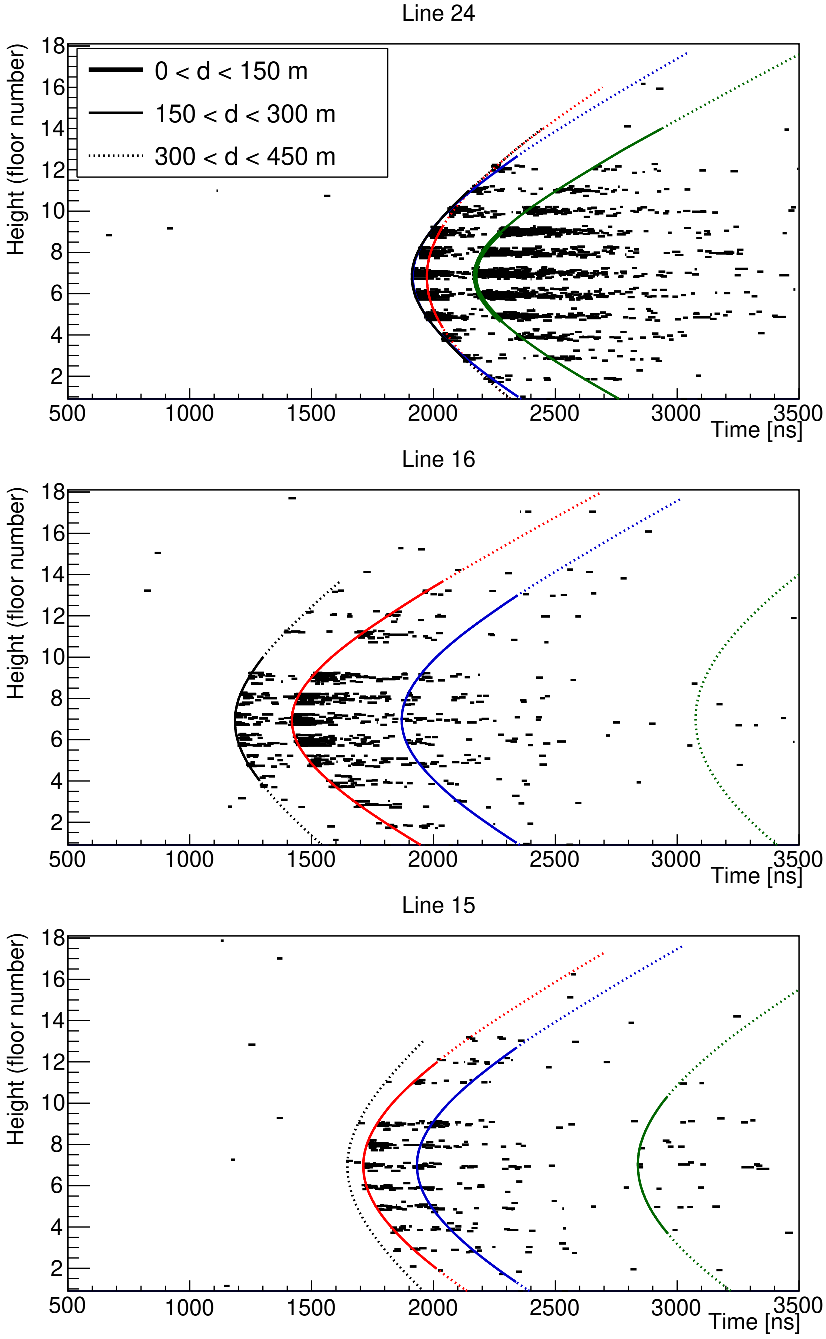

Supplementary Figure 2: Arrival times of the photons in KM3-230213A as a function of the height along three of the 21 detection lines. Each horizontal segment represents a detected PMT signal. The length of the line represents the amount of time during which the PMT signal is over threshold. The height in the detector is shown as the floor number, which indicates the optical module index (from 1, bottom, to 18, top). The curved lines indicate the expected light arrival time as a function of the height for light emitted from the muon (black) and from cascades located at $z = 199, 297$, and 477 m (red, blue and green, respectively). The style of the line indicates the distance d that the light needs to travel from the muon or the cascade as shown in the legend.

References

[1] R. Abbasi et al. (IceCube Collaboration), *Improved Characterization of the Astrophysical Muon–neutrino Flux with 9.5 Years of IceCube Data*, Astrophysical Journal **928** (1): 50, 2022, doi:10.3847/1538-4357/ac4d29

[2] R. Abbasi et al. (IceCube Collaboration), *Characterization of the astrophysical diffuse neutrino flux using starting track events in IceCube*, Physical Review D **110** (2): 022001, 2024, doi:10.1103/PhysRevD.110.022001

[3] R. Abbasi et al. (IceCube Collaboration), *The IceCube high-energy starting event sample: Description and flux characterization with 7.5 years of data*, Physical Review D **104**: 022002, 2021, doi:10.1103/PhysRevD.104.022002

[4] R. Aloisio, V. Berezinsky and P. Blasi, *Ultra high energy cosmic rays: implications of Auger data for source spectra and chemical composition*, Journal of Cosmology and Astroparticle Physics **10**: 020, 2014, doi:10.1088/1475-7516/2014/10/020

[5] M.S. Muzio, M. Unger and S. Wissel, *Prospects for joint cosmic ray and neutrino constraints on the evolution of trans-Greisen-Zatsepin-Kuzmin proton sources*, Physical Review D **107** (10): 103030, 2023, doi:10.1103/PhysRevD.107.103030

[6] D. Ehlert et al., *Constraints on the proton fraction of cosmic rays at the highest energies and the consequences for cosmogenic neutrinos and photons*, Journal of Cosmology and Astroparticle Physics **02**: 022, 2024, doi:10.1088/1475-7516/2024/02/022

[7] B.T. Zhang and K. Murase, *Ultrahigh-energy cosmic-ray nuclei and neutrinos from engine-driven supernovae*, Physical Review D **100** (10): 103004, 2019, doi:10.1103/PhysRevD.100.103004

[8] A. Abdul Halim et al. (Pierre Auger Collaboration), *Constraining the sources of ultra-high-energy cosmic rays across and above the ankle with the spectrum and composition data measured at the Pierre Auger Observatory*, Journal of Cosmology and Astroparticle Physics **05**: 024, 2023, doi:10.1088/1475-7516/2023/05/024,

[9] M.S. Muzio and G.R. Farrar, *Constraints on the Hosts of UHECR Accelerators*, Astrophysical Journal Letters **942** (2): L39, 2023, doi:10.3847/2041-8213/acac93

[10] D. Boncioli, D. Biehl and W. Winter, *On the common origin of cosmic rays across the ankle and diffuse neutrinos at the highest energies from low-luminosity Gamma-Ray Bursts*, Astrophysical Journal **872** (1): 110, 2019, doi:10.3847/1538-4357/aafda7

[11] J. Heinze et al., *A new view on Auger data and cosmogenic neutrinos in light of different nuclear disintegration and air-shower models*, Astrophysical Journal **873** (1): 88, 2019, doi:10.3847/1538-4357/ab05ce

[12] A. Condorelli et al., *Testing hadronic and photohadronic interactions as responsible for ultrahigh energy cosmic rays and neutrino fluxes from starburst galaxies*, Physical Review D **107** (8): 083009, 2023, doi:10.1103/PhysRevD.107.083009

[13] C. Berat et al., *Floor of Cosmogenic Neutrino Fluxes above 10^{17} eV*, Astrophysical Journal **966** (2): 186, 2024, doi:10.3847/1538-4357/ad372a

[14] K. Fang et al., *Testing the Newborn Pulsar Origin of Ultrahigh Energy Cosmic Rays with EeV Neutrinos*, Physical Review D **90** (10): 103005, 2014, doi:10.1103/PhysRevD.90.103005 [Erratum: Physical Review D **92**: 129901, 2015]

[15] X. Rodrigues et al., *Active Galactic Nuclei Jets as the Origin of Ultrahigh-Energy Cosmic Rays and Perspectives for the Detection of Astrophysical Source Neutrinos at EeV Energies*, Physical Review Letters **126** (19): 191101, 2021, doi:10.1103/PhysRevLett.126.191101

[16] W. Winter and C. Lunardini, *Interpretation of the Observed Neutrino Emission from Three Tidal Disruption Events*, Astrophysical Journal **948** (1): 42, 2023, doi:10.3847/1538-4357/acbe9e

[17] X. Rodrigues et al. *Leptohadronic multi-messenger modeling of 324 gamma-ray blazars*, Astronomy & Astrophysics **681**: A119, 2024, doi:10.1051/0004-6361/202347540

[18] I. Tamborra and S. Ando, *Diffuse emission of high-energy neutrinos from gamma-ray burst fireballs*, Journal of Cosmology and Astroparticle Physics **09**: 036, 2015, doi:10.1088/1475-7516/2015/9/036,